HHS Public Access

Author manuscript

Methods Enzymol. Author manuscript; available in PMC 2024 July 19.

Published in final edited form as:

Methods Enzymol. 2024 ; 701: 359–386. doi:10.1016/bs.mie.2024.03.028.

Free energy calculations for membrane morphological transformations and insights to physical biology and oncology

Kshitiz Parihar[a], **Seung-Hyun Ko**[b], **Ryan Bradley**[a], **Phillip Taylor**[a], **N. Ramakrishnan**[b], **Tobias Baumgart**[c], **Wei Guo**[d], **Valerie M. Weaver**[e], **Paul A. Janmey**[b,f], **Ravi Radhakrishna**[a,d,*]

[a]Department of Chemical and Biomolecular Engineering, School of Engineering and Applied Science, University of Pennsylvania, Philadelphia, PA, United States

[b]Department of Bioengineering, School of Engineering and Applied Science, University of Pennsylvania, Philadelphia, PA, United States

[c]Department of Chemistry, School of Arts & Sciences, University of Pennsylvania, Philadelphia, PA, United States

[d]Department of Biology, School of Arts & Sciences, University of Pennsylvania, Philadelphia, PA, United States

[e]Department of Surgery, Center for Bioengineering and Tissue Regeneration, University of California, San Francisco, San Francisco, CA, United States

[f]Department of Physiology, Perelman School of Medicine, University of Pennsylvania, Philadelphia, PA, United States

Abstract

In this chapter, we aim to bridge basic molecular and cellular principles surrounding membrane curvature generation with rewiring of cellular signals in cancer through multiscale models. We describe a general framework that integrates signaling with other cellular functions like trafficking, cell-cell and cell-matrix adhesion, and motility. The guiding question in our approach is: how does a physical change in cell membrane configuration caused by external stimuli (including those by the extracellular microenvironment) alter trafficking, signaling and subsequent cell fate? We answer this question by constructing a modeling framework based on stochastic spatial continuum models of cell membrane deformations. We apply this framework to explore the link between trafficking, signaling in the tumor microenvironment, and cell fate. At each stage, we aim to connect the results of our predictions with cellular experiments.

1. Mechanotransduction through membrane signalosomes

Formation of membrane signalosomes (i.e., signaling complexes that are central to intracellular trafficking), is coupled with specific and deliberate deformations of the cell membrane. Examples of such membrane-mediated processes include the formation of membrane structures (e.g., filopodia, lamellipodia, podosomes) that are required for cell

*Corresponding author.rradhak@seas.upenn.edu.

movement or survival, and various membrane-trafficking and recycling events on the plasma membrane and the endosome (e.g., endocytosis, exocytosis, phagocytosis). Collectively, these intracellular trafficking mechanisms involve the interactions between proteins and lipids and are crucial to essential cell functions, including nutrient uptake, cell motility, cell–cell communication, and cellular homeostasis. These intracellular transport mechanisms dynamically regulate and impact signaling by modulating receptor activity, and protein localization.

While the driving forces for the assembly of these functional signalosomes are not precisely understood, it is appreciated that the assembly itself requires an elaborate and delicate orchestration of multiple proteins and lipids in precise spatial patterns and temporal sequence. Interactions within the membrane signalosome for four trafficking classes (endocytosis, exocytosis, endosomal sorting, and exosome release) can be further classified into: protein signals, lipid signals, mechanical signals (e.g., curvature, tension, excess area, force, adhesion, line tension), and mechano-biochemical coupling (through membrane-cortex interactions) (Kutateladze, 2010). Changes in membrane stiffness, curvature, tension, and other mechanical factors, will alter the balance between these panoplies of interactions, thus biasing information-transfer pathways and influencing the nature of the signal. For example, they can serve to switch the signaling profile from one that promotes differentiation to one that promotes growth (Bissell & Hines, 2011).

Remodeling of membrane curvature is an essential part of several cellular processes ranging from cell division and motility to cargo trafficking and growth (Jarsch, Daste, & Gallop, 2016; McMahon & Boucrot, 2015). Among several mechanisms, curvature-inducing peripheral membrane proteins play a central role in membrane remodeling by asymmetrically engaging and crowding one side of the bilayer, thereby perturbing one of the leaflets and thus generating membrane curvature (Zimmerberg & Kozlov, 2006; Shibata et al., 2009; Kozlov et al., 2014). These curvature-inducing proteins are also capable of sensing both membrane curvature (Baumgart et al., 2011; Bhatia et al., 2009; Martyna et al., 2016; Tsai et al., 2021; Peter et al., 2004) and tension (Diz-Muñoz, Fletcher, & Weiner, 2013). This multifunctionality is thought to enable cells to use these proteins to sense curved regions to localize towards in order to further augment changes in membrane curvature. For instance, dynamin GTPases, key drivers of membrane scission (Ferguson & De Camilli, 2012), have been shown in vitro to favor binding on higher curvature membrane tubes as compared to liposomes (Roux et al., 2010). This property of dynamin as a curvature sensor provides a possible mechanism by which cells efficiently recruit dynamin proteins to the constricted neck region of mature clathrin-bound buds to induce membrane fission for detaching the vesicle (McDargh et al., 2016). We note that there are other mechanisms of inducing morphological transitions due to asymmetric crowding inducing a pressure differential across the bilayer that do not require curvature inducing proteins. Due to space limitations, we will not focus on the interesting literature on these systems and mechanisms, but we hope some of the methods described here can be leveraged to study them, as illustrated in recent work (Kandy & Radhakrishnan, 2022).

Unlike established methods in structural biology or optical microscopy, experimental protocols to study cell membrane-mediated trafficking are challenging and limited. The

relevant length scale (10–100 nm) for functional assemblies are too large for atomic resolution and yet fall below the diffraction limit to elude many optical methods. Yet, spatio-temporal orchestration of these functional protein-lipid assemblies transduces many incoming and outgoing cell signals, ultimately linking (and often governing) signal transduction to cell fate and function. Yet, principles surrounding such trafficking phenomena are rudimentary at best.

We advocate that integration of models from physical biology (e.g., cell membrane curvature, cytoskeletal tension and force, cell-matrix adhesion) and models from systems biology (e.g., signal transduction based on networks) can lead to quantitative paradigms of intracellular trafficking. This approach is complementary to, and imposes crucial constraints on, mechanisms gleaned from cell-based experiments. In light of the important role of these elementary cellular transport mechanisms, we focus on building a computational platform for constructing (minimal) models of such intracellular processes involving the membrane by integrating theoretical and computational approaches from statistical mechanics and soft condensed matter theory. The models described here are spatially resolved and stochastic, and simultaneously incorporate structural, energetic, and kinetic interactions. The models are validated through cellular experiments on cell membrane remodeling and trafficking (including experiments at the sub-optical resolution) and can be predictive in nature in terms of discovering “hidden” principles governing intracellular trafficking in mammalian cell physiology.

The models will be multiscale in nature and will need to integrate three techniques: namely, coarse-grained molecular dynamics, continuum simulations, and intracellular signaling/trafficking models, even though in the current chapter, we only describe the continuum simulations. Through the integration of theory (at the nano and the molecular scale) and experiment, considerable new insight can be gained into the various processes of intracellular trafficking with respect to structure, assembly, and mechanisms, from both biological and physical perspectives.

2. Computational methods

There are several theoretical and computational techniques for studying membrane morphological transformations at molecular and mesoscopic length scales. As we describe in sections below, we specifically focus on the dynamically triangulated Monte Carlo (DTMC) technique because it allows easy access to study nontrivial morphologies, easy implementation of biophysical drivers of curvature (such as curvature fields or crowding), and a direct route to computing free energies. This latter aspect is important as the threshold parameters which determine the morphological transitions are sensitive to energetic and entropic effects.

2.1 Mesoscale methods for simulating membrane deformations

At the micron scale, a cell and its internal organelles display amazing complexity in their shape and organization. We explore the physical properties of a biological membrane using the phenomenological Canham-Helfrich Hamiltonian (Helfrich, 1973; Safran, 1999), which in the discrete form is given by,

$$H_{el} = \frac{k}{2}\sum_{v=1}^{N_v}\left(2H_v - H_0(v)^2\right)A_v. \quad (1)$$

Here, the membrane is approximated to a two dimensional fluid, elastic sheet, with lateral dimensions large enough (cellular scale) to neglect its thickness. The phenomenological parameter κ is the bending rigidity, and the summation is over the vertices of a discretized (triangulated) membrane surface with index v, and A_v represents the area per vertex. The gauge invariant $H_v = (c_1 + c_2)/2$ is the mean curvature of the membrane at the vertex (v), where c_1 and c_2 are the two principal radii of curvatures, and $H_0(v)$ is the spontaneous curvature (magnitude of imposed deformation) imposed on the membrane at the vertex (v) by a curvature modulating factor, which in general denotes any heterogeneity in composition of the membrane.

Analytical and semi-analytical techniques are typically only practical when the membrane under investigation has a smooth, axisymmetric shape; this class of shapes encompasses only a few amongst the large set of naturally occurring membrane morphologies (Safran, 1999; Seifert, 1997). We overcome this problem and explore the entire conformational space, at the meso and continuum levels, using computations based on the DTMC techniques (Ramakrishnan, Sunil Kumar, & Radhakrishnan, 2014) which implement the discrete form given in Eq. (1). The original implementation of the DTMC was advanced by Gompper ad Kroll over 3 decades ago (Gompper & Kroll, 1994) and in the specific implementation we utilize, the mean curvature is obtained using an efficient method from computational geometry (Ramakrishnan, Sunil Kumar, & Ipsen, 2010). In addition to the elastic energy, we account for the self-avoidance of the vertices through a link potential.

The DTMC method has several advantages: (A) thermal fluctuations that play a key role in the self-organization of membranes are accounted for; (B) the fluidity of the membrane, which makes it different from other thin film systems, is preserved; (C) the membrane morphology can be irregular and the method easily generalizes to the high curvature limit, which is most relevant for cellular membranes. In DTMC, the thin sheet representing the middle plane of a membrane bilayer is discretized into N material points (vertices), denoted by $\left\{\vec{X}\right\}$, and interconnected by a set of triangles (faces), denoted by $\left\{\vec{T}\right\}$; with each triangle representing a planar membrane patch, with a characteristic length scale a_0, where a_0 is much greater than a lipid lengthscale. The triangulated membrane explores all accessible equilibrium states in its phase space, corresponding to a given thermodynamic state point. These moves (see Fig. 1, *left*)—(A) *vertex move*—the position of a randomly chosen vertex is perturbed around its mean position such that $\left\{\vec{X}\right\} \rightarrow \left\{\vec{X}'\right\}$ and (B) *link flip*—a link shared between two triangles is flipped by reconnecting the previously unshared vertices in the two triangles—are accepted using the Metropolis scheme with a probability given by the Boltzmann factor of the energy change associated with the move. Patches of the simulated membranes in the triangulated representation at different values of the excess areas (Aex) in the absence of spontaneous curvature are shown in Fig. 1 (*right*).

2.1.1 Constant projected area and constant frame tension ensembles—

In a simulated patch, it should be noted that the membrane projected area and surface area can be changed independently of each other. A membrane patch in our simulations is bounded and subjected to periodic boundary conditions by a square frame of size L that defines the projected area of the surface as $A_P = L^2$. An equilibrated membrane patch has a curvilinear area A_{mem} that is greater than A_p. To obtain a membrane patch subject to a range of different tension values, we construct systems with different A_{ex}. We initialize the membrane as a planar square grid with grid size l_0 and $50l_0 = L$. Each square is subdivided into two triangles with diagonal length $\sqrt{2}l_0$ to form a triangulated surface. This grid is then equilibrated using the MC procedure described above.

In a constant projected area ensemble, the various A_{ex} values are obtained by holding A_p constant (David & Leibler, 1991). Hence A_{ex} in the range of 2%–55% (see Fig. 1) is set by the choice of l_0. As an alternative to the constant projected area method, we can incorporate the frame tension explicitly through a constant frame tension ensemble, where we apply a frame tension to the membrane and allow the projected area A_p to fluctuate (Ramakrishnan et al., 2018).

2.2 Mesoscale methods for curvature inducing proteins on biological membranes

In this framework, we quantify the spontaneous curvature, induced by the membrane proteins, as curvature fields and study this phenomenon using two models (isotropic and anisotropic) as described below.

2.2.1 Isotropic elastic model—

In this approach, we consider membrane deformations due to curvature-inducing proteins through a curvature field using a functional form that is isotropic in the vicinity of the protein—in our studies we have chosen this form to be a Gaussian function with a range b_i and magnitude $C_{0,i}$, see Fig. 2. Hence the spontaneous curvature induced at a membrane vertex v due to the i^{th} protein at vertex v_i is:

$$H^e_{0,i}(v) = C_{0,i}\ \exp\left(\frac{(r_v - r_i)^2}{b_i^2}\right), \tag{2}$$

where r_i is the three-dimensional position vector of vertex v_i. The net induced curvature, due to N_e proteins, given by $\{\Phi\}$, is a superposition of these individual contributions,

$$H^e_0(v) = \sum_{i=1}^{N_e} H^e_{0,i}. \tag{3}$$

The parameters can be determined from experiments or through calculations (see our detailed estimates in (Tourdot et al., 2014a, 2015)): for example, by requiring that the membrane deformations promoted by the ENTH domain of the epsin protein be consistent

with experiments, we can determine $b_i = 8.3\,\mathrm{nm}$ and $C_0^i = 0.048\,\mathrm{nm}^{-1}$ (Tourdot et al., 2014a; Liu et al., 2012). The ENTH domain diffuses on the membrane manifold through an additional Monte Carlo move—where the hopping of a protein at a vertex v to any of its neighboring vertices is accepted using the Metropolis criterion. In addition to the mobile curvature-inducing proteins described above, a background curvature induced in the membrane (such as due to presence of a clathrin coat) is modeled as (Tourdot et al., 2014b; Liu et al., 2012):

$$H_0^c(v) = C_0 \Gamma(r_0), \tag{4}$$

where, $\Gamma(\mathrm{r}_0)$ is a function that is unity within a circular domain (centered at zero) of radius r_0 and zero otherwise; r_0 is the linear extent (radius) of the curvature-field induced by clathrin and C_0 is the magnitude of clathrin-induced curvature. Total energy of the system $\mathscr{H}_{\mathrm{tot}} = \mathscr{H}_{\mathrm{el}}$.

2.2.2 Anisotropic elastic model—Experimental studies on some classes of curvature-inducing domains containing peripheral proteins (Peter et al., 2004; Madsen et al., 2010; Masuda et al., 2006; Mim et al., 2012; Parthasarathy & Groves, 2007; Ren et al., 2006; Zimmerberg & McLaughlin, 2004) have suggested an anisotropic nature of the induced curvature field and these results have been complemented by computational studies (Mim et al., 2012; Anton, Ying, & Klaus, 2009; Arkhipov, Yin, & Schulten, 2008; Arkhipov, Yin, & Schulten, 2009; Yin, Arkhipov, & Schulten, 2009; Zhao et al., 2013), which also predict oligomerization of protein monomers and an orientational interactions between these units.

To account for this anisotropic phenomenon, we recast the protein into a nematic vector $\boldsymbol{n}$, which represents the orientation of proteins averaged over the membrane patch, associated with a triangle, see Fig. 3). The self-interaction of these nematic vectors are represented by the Lebwohl-Lasher form of the Frank free energy for liquid crystals given by (Lebwohl & Lasher, 1972),

$$H_{\mathrm{nem-nem}} = \frac{1}{2}\sum_{v=1}^{N_v}\sum_{v'=1}^{Z_v} -\varepsilon_{LL}\left(3\cos^2\theta_{vv'} - 1\right). \tag{5}$$

The first summation index v runs over all membrane vertices and v' runs over its Z_v neighboring vertices. ε_{LL} is the orientational stiffness and $\theta_{vv'}$ is the angle between $\boldsymbol{n}(\boldsymbol{v})$ and $\boldsymbol{n}(\boldsymbol{v}')$, computed on the curved manifold through a discrete parallel transport. $\boldsymbol{n}(\boldsymbol{v})$ is a two-dimensional unit vector confined to the surface of the membrane, as a protein does, and subtends an angle φ with the maximally curved direction of the membrane, as depicted in the left panel of Fig. 3.

We extend the Helfrich Hamiltonian, Eq. (1), to include the anisotropic curvature and account for the protein membrane interactions through an anisotropic energy term given by,

$$\mathscr{H}_{\text{nem-mem}} = \frac{1}{2}\sum_{v=1}^{N_v}\left\{\kappa_{\parallel}\left(c_1\cos^2\varphi + c_2\sin^2\varphi - H_0^{\parallel}\right)^2 + \kappa_{\perp}\left(c_1\sin^2\varphi + c_2\cos^2\varphi - H_0^{\perp}\right)^2\right\}A_v\,. \tag{6}$$

$\kappa_{\parallel}(\kappa_{\perp})$ and $H_0^{\parallel}(H_0^{\perp})$ are respectively the anisotropic bending stiffness and anisotropic spontaneous curvature parallel (perpendicular) to the nematic field $\boldsymbol{n}$. The nematic field evolves through a Monte Carlo move that perturbs the field orientation and the move is accepted using the Metropolis algorithm (see right panel in Fig. 3). The total energy of the membrane including the nematic field is $\mathscr{H}_{\text{tot}} = \mathscr{H}_{\text{el}} + \mathscr{H}_{\text{nem-nem}} + \mathscr{H}_{\text{nem-mem}}$.

2.3 Calculation of free energies for membranes with curvature protein fields

We have developed several strategies (Ramakrishnan et al., 2014; Tourdot et al., 2014a, 2014b, 2015; Agrawal & Radhakrishnan, 2009; Ramanan et al., 2011; Ramakrishnan, Tourdot, & Radhakrishnan, 2016) to compute the relative free energy changes when a curvature-inducing field binds to a membrane.

2.3.1 Widom insertion method—The chemical potential (μ_{ex}) to add a protein field to the membrane is given by,

$$\mu_{\text{ex}} = -k_B T \ln \int ds_{M+1} \langle \exp(-\beta \Delta \mathscr{H}_{\text{tot}}) \rangle_M\,. \tag{7}$$

For a membrane with M curvature-inducing sites with non-zero isotropic/anisotropic field, the ensemble average $\langle \exp(-\beta \Delta \mathscr{H}_{\text{tot}}) \rangle_N$ is computed by inserting a protein field at randomly chosen vertices on the membrane. Eq. (7) is integrating over the position of the $(m + 1)^{\text{th}}$ curvature field sampled as test insertion (or ghost insertion) when m fields are already present. Successful validation and application of this methodology was demonstrated in our recent published work (Tourdot et al., 2014b). Since, we have generalized the above framework for inhomogeneous systems, which show a spatial variation in protein density. This extension enables us to study curvature induced protein migration and track how local protein density tracks with local curvature.

2.3.2 Thermodynamic integration—In this method the free energy is coupled to a coupling parameter λ. The derivative of the Helmholtz free energy $F = -k_B T \ln Q$ (where Q is the partition function), can be written as:

$$\frac{\partial F}{\partial \lambda} = \left\langle \frac{\partial \mathscr{H}_{\text{tot}}}{\partial \lambda} \right\rangle, \tag{8}$$

and the free energy can be calculated as,

$$F\left(\kappa_{\parallel}, \kappa_{\perp}, \varepsilon_{LL}, H_0^{\parallel}, H_0^{\perp}\right) = \int_0^1 \left\langle \frac{\partial \mathscr{H}_{\text{tot}}}{\partial \lambda} \right\rangle d\lambda \,. \tag{9}$$

Eq. (9) is written for the anisotropic model based on the variables defined in Eq. (6). We have previously demonstrated the use of this method to compute relative free energies for a membrane surface coupled to intrinsic curvature-inducing fields when membrane curvature is small (Agrawal & Radhakrishnan, 2009). Subsequently, we have generalized this approach to membrane morphologies under high curvature such that they can be successfully applied to morphological transitions in cell membranes (such as vesiculation, tubulation, etc.) (Ramakrishnan et al., 2014; Tourdot et al., 2014a, 2014b). In the present studies, we couple the anisotropic stiffness to the parameter λ, such that $\kappa_{\parallel} \longrightarrow \lambda\kappa_{\parallel}, \kappa_{\perp} \longrightarrow \lambda\kappa_{\perp}$ and $\varepsilon_{LL} \longrightarrow \lambda\varepsilon_{LL}$ in Eq. (9). This approach gives us the flexibility to construct the free energy landscape in one-dimensional or multi-dimensional parameter space.

2.4 Implementation

Monte Carlo moves are implemented to attempt and accept vertex moves, link flips, and movement of curvature fields. In the case of the anisotropic model, moves for the rotation of the curvature fields are also implemented. The different moves are selected and attempted at random only specifying the overall percentage of each type of move.

Our implementation of the DTMC is not that different from the original implementation by Gompper and Kroll. The main difference as noted earlier is that the algorithm we use to compute the mean curvature is much more efficient, therefore speeding up computational time. The other key difference is that we predominantly simulate a membrane supported by a frame and hence the excess membrane area is determined by a frame tension. This differs from the original implementation which simulates closed surfaces under a present pressure differential.

In our implementation, a given membrane patch, typically consisting of 50 by 50 vertices with periodic boundaries in plane, independent simulations for 15 million Monte Carlo steps are performed and the statistics are converted to thermodynamic averages. Here, each MC step consists of attempting as many vertex moves as the number of vertices and as many link flips flipping as the number of links. The typical runtime for an umbrella-sampling window to sample 15 million Monte Carlo steps is around 360 h on a 2.6 GHz processor.

The free energy calculations using the Widom insertion method are implemented similar to the regular Monte Carlo run, with several ghost field insertions attempted at random in between the MC moves. The calculations involving thermodynamic integration are implemented by dividing the integration variable space into multiple windows (λ advanced from 0 to 1 in steps of 0.1) and the slope of the free energy with respect to that variable determined in each window; the integration is performed using Simpson's rule.

All of the stated free energy techniques involve sampling across a large number of intermediate states, which in a conventional HPC setup would require thousands of

computational cores. We leverage the large core architecture of the Intel Xeon phi coprocessors and perform the free energy calculations using the symmetric processing mode. We tested this idea on a 20-core node, which also contains two 7120 P Intel Xeon phi coprocessors each with 240 cores. We were able to successfully run our free energy calculations spread over 500 individual windows on a single node. Though the coprocessors are three times slower than the CPU cores, this allows us to pursue a computationally intense problem with optimal resources, which is otherwise computationally intractable even with traditional supercomputing platforms.

3. Applications in cellular biophysics

3.1 Applications of free energy methods to mesoscale model for intracellular trafficking

Using the machinery of DTMC simulations (Ramakrishnan et al., 2014, 2016): we compared two free-energy methods (Widom insertion and thermodynamic integration) to delineate the free-energy landscape of curvature-inducing proteins on bilayer membranes (Fig. 4). Our results demonstrate the utility of these methods in computing the excess chemical potentials associated with curvature-inducing proteins on the membrane—in particular, we use this method to track the onset of morphological transitions (tubulation on the membrane surface) in the membrane at elevated protein densities (Tourdot et al., 2014b). Our results showing an agreement between these two methods provide an internal validation of these independent approaches. Furthermore, the predictions from the Widom method have been tested against analytical calculations of the excess chemical potential at infinite dilution (data shown in (Tourdot et al., 2014b)). Our results are useful in precisely quantifying the free-energy landscape, and also in determining the phase boundaries associated with curvature-induction, curvature-sensing, and morphological transitions. This approach has also been extended by us to study the role of thermal fluctuations and other external (control) variables, such as membrane tension, in shaping curvature-mediated vesiculation on bilayer membranes (Tourdot et al., 2015) as we show below.

3.1.1 Clathrin-mediated endocytosis—We explored the roles of cooperative protein-protein and protein-membrane interactions in the ubiquitous endocytic pathway in mammalian cells, clathrin-mediated endocytosis (CME), using the isotropic curvature field model (Agrawal, Nukpezah, & Radhakrishnan, 2010) (Eqs. 2–4), see (Fig. 5). In our model for CME, the epsins bind to the lattice of a growing clathrin coat through the interaction of the CLAP domain of epsin with the clathrin triskelion. This way, multiple epsins localized spatially and orientationally templated on the clathrin coat collectively play the role of a curvature inducing capsid. In addition, epsin serves as an adapter in binding the clathrin coat to the membrane through the interaction of its ENTH domain with the lipid PI(4,5)P2 on the membrane.

We have also successfully extended these results to consider how thermal fluctuations influence the vesicle morphologies (Tourdot et al., 2014a; Liu et al., 2012), see Fig. 5. Through our results, we identified a unique dual role for the tubulating protein epsin: namely that of curvature induction and that of an adapter between clathrin coat and the membrane. Our results also suggested an important role for the clathrin lattice, namely in

the spatial- and orientational-templating of epsins. In particular, we suggest that there exists a critical size of the coat above which a vesicular bud with a constricted neck resembling a mature vesicle is stabilized (Agrawal et al., 2010). Without fitting, (i.e., based on direct estimation of parameters from independent experimental studies and CGMD simulations), the model reproduces the observed shapes of vesicular intermediates as well as their probability distributions quantitatively in wild-type as well as CLAP IgG injected neuronal cell experiments (Fig. 5); the physical differences in morphologies are cartooned below the histograms. Our results also quantify the effect of bending rigidity and interfacial tension on the stability and morphology of vesicle nucleation in CME (Tourdot et al., 2014a; Liu et al., 2012).

3.1.2 Membrane exvaginations induced by the exocyst complex—We have applied the anisotropic curvature model (Eqs. 5–6) in the DTMC simulations to the capture the collective role of Exo70 domains found in the Exocyst complex proteins in reshaping membranous vesicle. The wild type proteins when attached to the outer surface of giant unilamellar vesicles (GUVs) induce inward-growing tubes. This phenomenon is recapitulated in our simulations by choosing a negative value of $H_0^{\parallel}$ in our anisotropic curvature model. The result of this study comparing model and experiment is shown in Fig. 6) and described in detail in Zhao et al. (2013): in particular, the equilibrium membrane conformation stabilized in the model shows striking similarity to that obtained from experiments.

3.1.3 Vesicular budding due to membrane constriction by ESCRT proteins —The Endosomal Sorting Complexes Required for Transport (ESCRT) are a family of cytosolic proteins, which are known be involved in membrane budding and also in endosomal sorting. In vitro, it has been shown that ESCRT-I and ESCRT-II are enough to generate membrane buds that grow into the cytosolic side of a GUV (Hurley, 2008; Hurley & Hanson, 2010; Im et al., 2009; Wollert & Hurley, 2010; Wollert et al., 2009). In experiments, it has been observed that the ESCRT proteins are localized to the neck region of the budded vesicle; in Fig. 7) (left) green regions represent the ESCRT proteins in the experimental data taken from Hurley and Hanson (2010). Beyond the puzzle of just being localized at the neck and induce vesiculation, available experimental evidence suggests that these proteins may actually induce a range of vesicle diameters from 30–150 nm in response to PI3P binding. No known mechanisms exist to explain these observations. In our earlier studies using the isotropic curvature model, see section on Clathrin-Mediated Endocytosis, it has been shown that bud formation requires the presence of an induced curvature field in the budding region. The absence of the ESCRT proteins on the surface of the bud, throughout the experiment, rules out such a phenomenon.

Using the anisotropic curvature model and localizing the protein curvature field to an annular region we demonstrate a novel phenomenon where a negatively curved vesicular bud is formed due to the constrictive action of either positively or negatively curving proteins, localized in an annular region around the neck. The bud is stabilized for curvature fields above a critical threshold value of $H_0^{\parallel} = -0.6/l_0$ (parameter defined in Eq. 6) and at a critical size of the annular region, see Fig. 7. We also observe that the annulus like arrangement

of the curvature field is unstable below a lower threshold while it prefers to segregate to a single patch when the surface coverage exceeds an upper threshold. Our results suggest an intricate balance between the entropy of localizing proteins to an annulus and the free energy of stabilizing a vesicle. To address this subject head-on, a detailed quantitative analysis of the thermodynamic stability of the annular distribution of the curvature field was performed, in order to directly relate to experiments and for predicting the concentration of the curvature remodeling members of the ESCRT family around the neck of the vesicle.

3.2 Cortical actin tension modulates plasma membrane topology

Cortical actin regulates membrane protrusions through physical attachments to the membrane and by doing so influences membrane topology (Bisaria et al., 2020). Membrane topology regulates the binding of curvature-associated proteins that reinforce membrane organization and influence cell signaling and the trafficking of cellular proteins including their recycling and secretion (Jarsch et al., 2016). Consistent with these actin-regulated membrane phenotypes, inhibiting actomyosin tension in the mammary epithelial cells engaging the etracellular matrix (ECM) in two-dimensions (2D) increased recycling and secretion (marked by the protein SEC61 expression), suggesting cortical actin tension regulates secretory protein translocation into the lumen of the endoplasmic reticulum.
To address whether the context of ECM engagement influences protein secretion by regulating cortical actin tension-dependent membrane topology we used DTMC simulations to explore the morphological conformational space of planar to highly curved membranes (Ramakrishnan et al., 2014; Tourdot et al., 2014a, 2014b). Using this framework, we quantified the surface deformations induced by membrane proteins as curvature fields and studied the emergent morphologies of the membrane using isotropic and anisotropic curvature models. We simulated membrane patches with different excess area (A/A_p), which is the variable conjugate to the frame tension and depends on cortical actin tension (Ramakrishnan et al., 2018). Our free energy simulations for the formation of cellular protrusions were computed from the Helmholtz free energy change of the protrusion assembly (ΔF) and were plotted as a function of membrane excess area. The model predicted that the protrusions that assemble in the mammary epithelial cells engaging the ECM in 2D that experience high membrane tension (reflecting high cortical actin tension), herein depicted as being under small excess area (A/A_p), would be shorter and/or more transient. By contrast, the model indicated that the membrane protrusions that assemble in the same cells engaging the ECM in 3D, that experience low frame tension (reflecting lower cortical actin tension), would be longer and/or more stable. Consistent with these predictions, live cell microscopy showed that the cells interacting with the ECM in 2D formed highly dynamic, short membrane protrusions, whereas the cells interacting with ECM in 3D formed longer and more stable protrusions, quantified as increased protrusion length and residence time.

3.3 Cortical actin tension modulates plasma membrane protein composition

Plasma membrane protrusions are cylindrically shaped structures composed of a protrusion, an annulus and a basal component that combine to generate negative and positive curvature in the associated membrane. While the neck or annulus of the protrusion generates positive membrane curvature, the entire cytoplasmic length of the protrusion compartment

generates a negatively curved membrane. Membrane curvature regulates the binding affinity of membrane curvature-associated proteins that can exert profound effects on cell behaviors including endocytosis, protein secretion and recycling, organelle function and actin dynamics (McMahon & Boucrot, 2015). To explore the relationship between cortical actin tension, plasma membrane protrusions and plasma membrane topology, we extended our DTMC model to predict protein recruitment. We computed the excess chemical potential (or the free energy to add/recruit a protein) to these three spatial regions of the membrane (protrusion, annulus, and basal) as a function of membrane area (A/A_p) (proxy for cortical actin tension). Our calculations revealed that a lower value of the excess chemical potential signifies the favorable recruitment of a protein to a given membrane location and curvature to enhance its local protein density. Our computational analysis also revealed that the excess chemical potential of negative curvature-binding protein domains is preferentially localized to the cytosolic site of the membrane protrusions and predicted that this protein domain binding behavior will segregate more favorably under conditions of low membrane tension (cortical actin tension; 3D). Our energetics calculations further predicted that conditions in which cell tension is low (low membrane tension/low cortical actin tension; MECs engaging the ECM in 3D), the recruitment of positive curvature-inducing proteins would be hindered.

Given that Exo70 is a negative curvature binding/inducing protein that is also a component of the exocyst complex targeting secretory vesicles to the plasma membrane, we predicted that Exo70 could be a candidate protein regulated by cortical actin tension to facilitate secretory protein trafficking (Zhao et al., 2013). Consistent with our energetics model prediction, fluorescently-tagged Exo70 showed greater plasma membrane localization in the MECs engaging the ECM in 3D (low membrane/cortical actin tension) as revealed by a strong co-localization of the EGFP-Exo70 with membrane-tagged farnesylated mCherry as compared to minimal membrane associations observed in the MECs engaging the ECM in 2D. Reducing myosin activity in the MECs engaging the ECM in 2D (treatment with the inhibitor, blebbistatin) to recapitulate the membrane protrusion behavior of the MECs engaging the ECM in 3D, significantly enhanced the level of plasma membrane-associated Exo70, implicating cortical actin tension in this plasma membrane phenotype. The data suggest cortical actin tension could regulate secretory protein trafficking to the plasma membrane by regulating plasma membrane protrusion activity and topology.

The increased AnxA2 and Exo70 plasma membrane localization we observed is not only consistent with the DTMC simulations that predicted the plasma membrane binding of negative curvature-binding proteins, such as AnxA2 and Exo70, but also suggested that this binding could induce and stabilize negative plasma membrane curvature (Zhao et al., 2013; Boye et al., 2018). Accordingly, the findings suggest that cortical actin tension regulates membrane protrusion activity and plasma membrane topology to modulate the spatial distribution of negative curvature-binding proteins implicated in secretory protein trafficking.

3.4 Ultrasensitive response of vesiculation to changes in cortical tension

We then employed DTMC simulations to delineate how membrane deformations (such as vesiculation and tubulation) orchestrated by curvature-inducing proteins depend on

tension due to cytoskeleton. This connection between cortical tension and vesicle biogenesis confers an intriguing paradigm of mechanosensitivity to cellular functions and further underscores the need for considering biophysical effects on signaling pathways, to gain a holistic understanding of how mechanical stimuli such as ECM stiffening aid in tumor initiation and progression. In Section 3 earlier, we described key features in the curvature generation mechanism is the spatial localization of functional units via oligomerization and via membrane-mediated forces for inducing sufficient curvature followed by self-assembly of these functional units on the membrane to generate macroscopic high curvature morphologies like vesiculation and tubulation. DTMC simulations have revealed a micellization-like mechanism for membrane tubulation, wherein tubes formed by self-assembly of curvature-inducing proteins are analogous to micelle aggregates formed by self-assembly of surfactant molecules (Tourdot et al., 2015).

In cells, the deformation of a patch of membrane is also dependent on the cortical actin tension due to the associated cortex (Diz-Muñoz et al., 2013; Granger et al., 2014). To address how the curvature generating capabilities of curvature-inducing proteins is affected by cortical tension, we used DTMC simulations to explore the morphological conformational space of planar to highly curved membranes (Ramakrishnan et al., 2014; Tourdot et al., 2014a, 2015). The dependence of cortical tension is incorporated by simulating membrane patches with different A_{ex} (A/A_p, A is the curvilinear area of the membrane patch, and A_p is the projected area) where increasing excess area corresponds to decreasing cortical tension (Ramakrishnan et al., 2018). We analyzed how the membrane morphology changes with increasing excess area for a given total number of protein-induced curvature fields (n_p). The extent of curvature change can be seen in terms of how many protein fields are in the tubular region (n_t) for the equilibrium membrane morphologies. The equation for describing the simulation data (n_t vs $/A_p$) was obtained by generalizing the micelle model proposed in (Tourdot et al., 2015) and is given by:

$$n_t = a + \frac{b}{c + \left(\frac{A}{A_p} - 1\right)^n} \tag{10}$$

where a, b, and c are constants for a given n_p. The parameter n can be viewed as a Hill-type coefficient indicating cooperativity between protein fields to induce tubulation. For a fixed value of n, Eq. (10) was fitted to the data (n_t vs A/A_p) obtained from simulations for different n_p values. Eq. (10) with $n = 4$ yielded an optimal representation to fit the data. It is important to note the micellization based model used as the basis for Eq. (10) which underscores an interesting proposition wherein the ability of curvature-inducing proteins to self-assemble for formation of membrane protrusions is modulated by cortical tension. Hence, the Hill function-like dependence of curvature generation on excess area (proxy for cortical tension) suggests that lower cortical tension increases the tendency for curvature-inducing proteins to congregate and thereby, promotes morphological changes such as tubulation and vesiculation. The Hill-type ultrasensitivity suggests that the effect of cortical tension on

membrane deformation is captured by the change in the propensity of curvature-inducing proteins to self-assemble on the membrane for generating high curvature structures.

Our model predicts that a decrease in cortical tension could facilitate the creation of trafficking vesicles. However, increasing cortical tension does not necessarily mean a decrease in curvature induced by proteins, as the cortical tension increase could be within the saturation region of Hill-type dependence. This dependency suggests that the influence of ECM stiffness on membrane deformation depends on which region (saturated or sensitive) of the Hill-type function and by how much the cortical tension changes, which would be dependent on the cell type. For instance, an increase in cortical tension with stiffening ECM could be within the saturation region and thereby, not significantly affect the generation of highly curved structures.

4. Insights to cancer biophysics and oncology

A correlation exists between cancer cell mutations which confer fitness advantage to cells with a gain of basic cellular functions like cell adhesion and motility, signaling, transcriptional regulation and intracellular trafficking. Defective signaling and vesicular trafficking of growth factor receptors and their subsequent alteration of cell fate by influencing the downstream signaling pathways have been found to be the hallmark of cancer cell (Mosesson, Mills, & Yarden, 2008). The central goal of cancer biology is to find a mechanistic link between the above two factors, which has important implications in biomarker development and therapeutic efficacy. The central goal of oncology is to translate these findings into treatment regimens where optimization of therapeutic regimens can be customized to the genetic and physiological make-up of individualized patients or patient cohorts.

Metastatic cancer is a major clinical challenge that accounts for over 500,000 deaths per year in the United States of America (Wang et al., 2017; Kamangar, Dores, & Anderson, 2006; Luchini, Capelli, & Scarpa, 2016; Weigelt, Peterse, Van, & Veer, 2005). Delineating mechanisms would identify actionable biomarkers and novel therapeutic targets. Tumors develop within a cellular microenvironment characterized by altered ECM stiffness and composition, blood vessel architecture, and immune cell interactions. These microenvironment components play a causal role in tumor amplification and metastasis (Awaji & Singh, 2019; Dougan, 2017; Kai, Drain, & Weaver, 2019; Thomas & Radhakrishnan, 2019). The immune cells that are initially recruited to the tumor are anti-tumorigenic; however, as malignancy proceeds, shift towards a pro-tumor phenotype. Also, the frequency of the tumor-infiltrating immune cells becomes severely reduced. The reprogramming of immune cells to a pro-tumor phenotype and immune cell depletion and exhaustion are traits associated with an aggressive metastatic tumor (Allard et al., 2018; Binnewies et al., 2018; Burugu, Asleh-Aburaya, & Nielsen, 2017; Cotechini, Medler, & Coussens, 2015; Flores-Borja et al., 2016; Law et al., 2017; Padoan, Plebani, & Basso, 2019; Quigley & Kristensen, 2015; Ruffell & Coussens, 2015; Vitale et al., 2019; Broz & Krummel, 2015).

A stiff ECM and cytoskeletal tension promote tumor cell growth and survival and stimulate tumor cell invasion in culture (Dupont et al., 2011; Guilluy et al., 2011; Ishihara et al., 2017; Laklai et al., 2016; Levental et al., 2009; Miroshnikova et al., 2017; Mouw et al., 2014; Paszek et al., 2014). Studies in vivo using genetically engineered mouse models demonstrated that stiff ECM promotes malignant transformation (Levental et al., 2009; Egeblad, Rasch, & Weaver, 2010; Feig et al., 2012; Hewitt et al., 1993; Lu et al., 2011; Lu, Weaver, & Werb, 2012; Rubashkin et al., 2014). Recently exosomes have drawn tremendous interest in cancer research as tumor-derived exosomes ("TEXs") are implicated in modulating the tumor microenvironment, suppressing anti-tumor immunity, and preparing the metastatic niche for progression (Fig. 8) (Chen et al., 2018; Kurywchak, Tavormina, & Kalluri, 2018; Kalluri, 2016; Bae, Brumbaugh, & Bonavida, 2018; Nabet et al., 2017; Gao et al., 2018; Hoshino et al., 2015; Becker et al., 2016; Whiteside, 2016a; Xu et al., 2018). A major question in the field is: how are the release and composition of tumor exosomes regulated? How does tissue mechanics regulate cell cortical tension to influence exosome production and cargo composition by co-opting the biophysics as well as the signaling dynamics of intracellular trafficking pathways discussed in Section 3? And how do these exosomes contribute to the suppression of anti-tumor immunity and promote metastasis? Below, we provide experimental references and contexts adjacent to the computational work described in Section 3 to connect the computational results to studies that establish relevance to cancer mechanisms. The motivation is to demonstrate the direct applicability of findings from membrane simulations to help guide the search for mechanisms in the experimental studies.

The extracellular matrix influences cellular stress in breast or mammary epithelial cells (Kai et al., 2022): experimentally, it was observed that cells within a three dimensional laminin-rich extracellular matrix decreased and redistributed the actin crosslinker filamin to reduce their cortical actin tension compared to matrix contacting the cell in two-dimensions. Cells with low filamin-mediated cortical actin tension and reduced endoplasmic reticulum stress response signaling secreted, and assembled, a polarized endogenous basement membrane and survived better, under chemotherapeutic and radiation doses, and their spheroids were more resistant to exogenous stress. These results lead to the conclusion that ECM dimensionality tunes actomyosin tension to modulate cellular stress.

One of the main findings of the application described on Section 3 is that the link between the dimensionality of ECM engagement and cell survival is potentiated by trafficking vesicles. TEXs have been implicated in cancer progression and metastasis (Whiteside, 2016b), with studies showing their role in promoting tumor cell invasion (Hoshino et al., 2013) and migration (Sung et al., 2015) as well as helping establish pre-metastatic niches at distant tissue sites (Peinado et al., 2017). TEXs are also a vital component of the ability of cancer cells to evade the immune system (Chen et al., 2018; Kurywchak et al., 2018; Shinohara et al., 2017). The abnormally altered ECM stiffness observed in tumorigenesis and the dependence of cytoskeletal dynamics on matrix elasticity suggest a mechanosensitive mechanism employed by tumors for regulating trafficking pathways establishing a causal link between ECM stiffness and regulation of trafficking vesicles (Parihar et al., 2022).

A definitive understanding of the interplay between protein binding/migration and membrane curvature evolution is emerging but remains incomplete. Though aspects of these fundamental processes are well-characterized from a molecular biology perspective, especially in the domain of protein-protein interactions and increasingly in the area of protein localization, several open questions remain which are fundamental to a complete understanding of the underlying mechanisms in these fundamental unit cellular process from both a biophysical and thermodynamic perspective.

The effect of the proposed models go beyond fundamental investigation of specific cellular processes towards actual clinical trials. Exosomal mechanisms are critical to the development and approval of liquid biopsy technologies, which are slated to be the future of non-invasive, longitudinal profiling of evolving tumors and resistance to therapies in cancer patients to bring us one step closer to the promise of personalized medicine (Ignatiadis, Sledge, & Jeffrey, 2021). Moreover, delineation of mechanobiological regulation of exosomes are critical to our understanding of the evolution of solid tumors under physical stress from ECM and the interaction of tumor with the immune system, which makes it central for therapy, including immunotherapy. Already, clinical studies have revealed that exosomal profiling can classify responders and non-responders to immunotherapy in treatment of some solid cancers (Chen et al., 2018).

Acknowledgments

We thank members of the Guo, Weaver, Radhakrishnan, and Janmey Labs for insightful discussions related to the topics covered in this chapter. This study has received funding from the National Institutes of Health under R35GM136259 and U01CA250044. PAJ was also supported by the National Cancer Institute and Leidos Biomedical Research, Inc. under contract 15 × 008 with Frederick National Laboratory for Cancer Research. Computational resources were available in part from the extreme science and engineering discovery environment under grant MCB200101.

References

Agrawal NJ, Nukpezah J, & Radhakrishnan R (2010). Minimal mesoscale model for protein-mediated vesiculation in clathrin-dependent endocytosis. PLoS Computational Biology, 6(9), e1000926. [PubMed: 20838575]

Agrawal NJ, & Radhakrishnan R (2009). Calculation of free energies in fluid membranes subject to heterogeneous curvature fields. Physical Review E, Statistical, Nonlinear, and Soft Matter Physics, 80(1 Pt 1), 011925. [PubMed: 19658747]

Allard B, et al. (2018). Immuno-oncology-101: Overview of major concepts and translational perspectives. Seminars in Cancer Biology, 52(Pt 2), 1–11.

Anton A, Ying Y, & Klaus S (2009). Membrane-bending mechanism of amphiphysin N-BAR domains. Biophysical Journal, 97(10), 2727–2735. [PubMed: 19917226]

Arkhipov A, Yin Y, & Schulten K (2008). Four-scale description of membrane sculpting by BAR domains. Biophysical Journal, 95(6), 2806–2821. [PubMed: 18515394]

Arkhipov A, Yin Y, & Schulten K (2009). Membrane-bending mechanism of amphiphysin N-BAR domains. Biophysical Journal, 97(10), 2727–2735. [PubMed: 19917226]

Awaji M, & Singh RK (2019). Cancer-associated fibroblasts' functional heterogeneity in pancreatic ductal adenocarcinoma. Cancers (Basel), 11(3).

Bae S, Brumbaugh J, & Bonavida B (2018). Exosomes derived from cancerous and non-cancerous cells regulate the anti-tumor response in the tumor microenvironment. Genes Cancer, 9(3–4), 87–100. [PubMed: 30108680]

Baumgart T, et al. (2011). Thermodynamics and mechanics of membrane curvature generation and sensing by proteins and lipids. Annual Review of Physical Chemistry, 62, 483–506.

Becker A, et al. (2016). Extracellular vesicles in cancer: Cell-to-cell mediators of metastasis. Cancer Cell, 30(6), 836–848. [PubMed: 27960084]

Bhatia VK, et al. (2009). Amphipathic motifs in BAR domains are essential for membrane curvature sensing. Embo Journal, 28(21), 3303–3314. [PubMed: 19816406]

Binnewies M, et al. (2018). Understanding the tumor immune microenvironment (TIME) for effective therapy. Nature Medicine, 24(5), 541–550.

Bisaria A, et al. (2020). Membrane-proximal F-actin restricts local membrane protrusions and directs cell migration. Science (New York), 368(6496), 1205–1210.

Bissell MJ, & Hines WC (2011). Why don't we get more cancer? A proposed role of the microenvironment in restraining cancer progression. Nature Medicine, 17(3), 320–329.

Boye TL, et al. (2018). Annexins induce curvature on free-edge membranes displaying distinct morphologies. Scientific Reports, 8(1), 10309. [PubMed: 29985397]

Broz ML, & Krummel MF (2015). The emerging understanding of myeloid cells as partners and targets in tumor rejection. Cancer Immunology Research, 3(4), 313–319. [PubMed: 25847968]

Burugu S, Asleh-Aburaya K, & Nielsen TO (2017). Immune infiltrates in the breast cancer microenvironment: Detection, characterization and clinical implication. Breast Cancer (Tokyo, Japan), 24(1), 3–15. [PubMed: 27138387]

Chen G, et al. (2018). Exosomal PD-L1 contributes to immunosuppression and is associated with anti-PD-1 response. Nature, 560(7718), 382–386. [PubMed: 30089911]

Cotechini T, Medler TR, & Coussens LM (2015). Myeloid cells as targets for therapy in solid tumors. Cancer Journal (Sudbury, Mass), 21(4), 343–350. [PubMed: 26222088]

David F, & Leibler S (1991). Vanishing tension of fluctuating membranes. Journal of Physics II France, 1(8), 959–976.

Diz-Muñoz A, Fletcher DA, & Weiner OD (2013). Use the force: Membrane tension as an organizer of cell shape and motility. Trends in Cell Biology, 23(2), 47–53. [PubMed: 23122885]

Dougan SK (2017). The pancreatic cancer microenvironment. Cancer Journal (Sudbury, Mass), 23(6), 321–325. [PubMed: 29189327]

Dupont S, et al. (2011). Role of YAP/TAZ in mechanotransduction. Nature, 474(7350), 179–183. [PubMed: 21654799]

Egeblad M, Rasch MG, & Weaver VM (2010). Dynamic interplay between the collagen scaffold and tumor evolution. Current Opinion in Cell Biology, 22(5), 697–706. [PubMed: 20822891]

Feig C, et al. (2012). The pancreas cancer microenvironment. Clinical Cancer Research: An Official Journal of the American Association for Cancer Research, 18(16), 4266–4276. [PubMed: 22896693]

Ferguson SM, & De Camilli P (2012). Dynamin, a membrane-remodelling GTPase. Nature Reviews Molecular Cell Biology, 13(2), 75–88. [PubMed: 22233676]

Flores-Borja F, et al. (2016). Crosstalk between innate lymphoid cells and other immune cells in the tumor microenvironment. Journal of Immunology Research, 2016, 7803091. [PubMed: 27882334]

Gao L, et al. (2018). Tumor-derived exosomes antagonize innate antiviral immunity. Nature Immunology, 19(3), 233–245. [PubMed: 29358709]

Gompper G, & Kroll DM (1994). Phase diagram of fluid vesicles. Physical Review Letters, 73, 2139. [PubMed: 10056981]

Granger E, et al. (2014). The role of the cytoskeleton and molecular motors in endosomal dynamics. Seminars in Cell & Developmental Biology, 31, 20–29. [PubMed: 24727350]

Guilluy C, et al. (2011). The Rho GEFs LARG and GEF-H1 regulate the mechanical response to force on integrins. Nature Cell Biology, 13(6), 722–727. [PubMed: 21572419]

Helfrich W (1973). Elastic properties of lipid bilayers—Theory and possible experiments. Zeitschrift für Naturforschung C, 28(11–1), 693–703.

Hewitt RE, et al. (1993). Desmoplasia and its relevance to colorectal tumour invasion. International Journal of Cancer. 53(1), 62–69. [PubMed: 7677932]

Hoshino A, et al. (2015). Tumour exosome integrins determine organotropic metastasis. Nature, 527(7578), 329–335. [PubMed: 26524530]

Hoshino D, et al. (2013). Exosome secretion is enhanced by invadopodia and drives invasive behavior. Cell Reports, 5(5), 1159–1168. [PubMed: 24290760]

Hurley JH (2008). ESCRT complexes and the biogenesis of multivesicular bodies. Curr Opin Cell Biol, 20(1), 4–11. 10.1016/j.ceb.2007.12.002. [PubMed: 18222686]

Hurley JH, & Hanson PI (2010). Membrane budding and scission by the ESCRT machinery: It's all in the neck. Nature, 11(8), 556–566.

Ignatiadis M, Sledge GW, & Jeffrey SS (2021). Liquid biopsy enters the clinic—Implementation issues and future challenges. Nature Reviews Clinical Oncology, 18(5), 297–312.

Im YJ, et al. (2009). Structure and function of the ESCRT-II-III interface in multi-vesicular body biogenesis. Developmental Cell, 17(2), 234–243. [PubMed: 19686684]

Ishihara S, et al. (2017). Mechano-signal transduction in mesenchymal stem cells induces prosaposin secretion to drive the proliferation of breast cancer cells. Cancer Research, 77(22), 6179–6189. [PubMed: 28972074]

Jarsch IK, Daste F, & Gallop JL (2016). Membrane curvature in cell biology: An integration of molecular mechanisms. The Journal of Cell Biology, 214(4), 375–387. [PubMed: 27528656]

Kai F, Drain AP, & Weaver VM (2019). The extracellular matrix modulates the metastatic journey. Developmental Cell, 49(3), 332–346. [PubMed: 31063753]

Kai F, et al. (2022). ECM dimensionality tunes actin tension to modulate endoplasmic reticulum function and spheroid phenotypes of mammary epithelial cells. The EMBO Journal, 41(17), e109205. [PubMed: 35880301]

Kalluri R (2016). The biology and function of exosomes in cancer. The Journal of Clinical Investigation, 126(4), 1208–1215. [PubMed: 27035812]

Kamangar F, Dores GM, & Anderson WF (2006). Patterns of cancer incidence, mortality, and prevalence across five continents: Defining priorities to reduce cancer disparities in different geographic regions of the world. Journal of Clinical Oncology: Official Journal of the American Society of Clinical Oncology, 24(14), 2137–2150. [PubMed: 16682732]

Kandy SK, & Radhakrishnan R (2022). Crowding-induced membrane remodeling: Interplay of membrane tension, polymer density, architecture. Biophysical Journal, 121(19), 3674–3683. [PubMed: 35619564]

Kozlov MM, et al. (2014). Mechanisms shaping cell membranes. Current Opinion in Cell Biology, 29, 53–60. [PubMed: 24747171]

Kurywchak P, Tavormina J, & Kalluri R (2018). The emerging roles of exosomes in the modulation of immune responses in cancer. Genome Medicine, 10(1), 23. [PubMed: 29580275]

Kutateladze TG (2010). Translation of the phosphoinositide code by PI effectors. Nature Chemical Biology, 6(7), 507–513. [PubMed: 20559318]

Laklai H, et al. (2016). Genotype tunes pancreatic ductal adenocarcinoma tissue tension to induce matricellular fibrosis and tumor progression. Nature Medicine, 22(5), 497–505.

Law AM, et al. (2017). The innate and adaptive infiltrating immune systems as targets for breast cancer immunotherapy. Endocrine-Related Cancer, 24(4), R123–R144. [PubMed: 28193698]

Lebwohl PA, & Lasher G (1972). Nematic-liquid-crystal order—Monte-carlo calculation. Physical Review A, 6(1), 426–429.

Levental KR, et al. (2009). Matrix crosslinking forces tumor progression by enhancing integrin signaling. Cell, 139(5), 891–906. [PubMed: 19931152]

Liu J, et al. (2012). Mesoscale simulations of curvature-inducing protein partitioning on lipid bilayer membranes in the presence of mean curvature fields. Molecular Physics, 110(11–12), 1127–1137. [PubMed: 26500377]

Luchini C, Capelli P, & Scarpa A (2016). Pancreatic ductal adenocarcinoma and its variants. Surgical Pathology Clinics, 9(4), 547–560. [PubMed: 27926359]

Lu P, et al. (2011). Extracellular matrix degradation and remodeling in development and disease. Cold Spring Harbor Perspectives in Biology, 3(12).

Lu P, Weaver VM, & Werb Z (2012). The extracellular matrix: A dynamic niche in cancer progression. The Journal of Cell Biology, 196(4), 395–406. [PubMed: 22351925]

Madsen KL, et al. (2010). BAR domains, amphipathic helices and membrane-anchored proteins use the same mechanism to sense membrane curvature. FEBS Letters, 584(9), 1848–1855. 10.1016/j.febslet.2010.01.053. [PubMed: 20122931]

Martyna A, et al. (2016). Curvature sensing by a viral scission protein. Biochemistry, 55(25), 3493–3496. [PubMed: 27299375]

Masuda M, et al. (2006). Endophilin BAR domain drives membrane curvature by two newly identified structure-based mechanisms. The EMBO Journal, 25(12), 2889–2897. [PubMed: 16763557]

McDargh ZA, et al. (2016). Constriction by dynamin: Elasticity versus adhesion. Biophysical Journal, 111(11), 2470–2480. [PubMed: 27926848]

McMahon HT, & Boucrot E (2015). Membrane curvature at a glance. Journal of Cell Science, 128(6), 1065–1070. [PubMed: 25774051]

Mim C, et al. (2012). Structural basis of membrane bending by the N-BAR protein endophilin. Cell, 149(1), 137–145. [PubMed: 22464326]

Miroshnikova YA, et al. (2017). alpha5beta1-Integrin promotes tension-dependent mammary epithelial cell invasion by engaging the fibronectin synergy site. Molecular Biology of the Cell, 28(22), 2958–2977. [PubMed: 28877984]

Mosesson Y, Mills GB, & Yarden Y (2008). Derailed endocytosis: An emerging feature of cancer. Nature Reviews Cancer, 8(11), 835–850. [PubMed: 18948996]

Mouw JK, et al. (2014). Tissue mechanics modulate microRNA-dependent PTEN expression to regulate malignant progression. Nature Medicine, 20(4), 360–367.

Nabet BY, et al. (2017). Exosome RNA unshielding couples stromal activation to pattern recognition receptor signaling in cancer. Cell, 170(2), 352–366.e13. [PubMed: 28709002]

Padoan A, Plebani M, & Basso D (2019). Inflammation and pancreatic cancer: Focus on metabolism, cytokines, and immunity. International Journal of Molecular Science, 20(3).

Parihar K, et al. (2022). Data driven and biophysical insights into the regulation of trafficking vesicles by extracellular matrix stiffness. Iscience, 25(8).

Parthasarathy R, & Groves JT (2007). Curvature and spatial organization in biological membranes. Soft Matter, 3(1), 24–33.

Paszek MJ, et al. (2014). The cancer glycocalyx mechanically primes integrin-mediated growth and survival. Nature, 511(7509), 319–325. [PubMed: 25030168]

Peinado H, et al. (2017). Pre-metastatic niches: Organ-specific homes for metastases. Nature Reviews Cancer, 17(5), 302–317. [PubMed: 28303905]

Peter BJ, et al. (2004). BAR domains as sensors of membrane curvature: The amphiphysin BAR structure. Science (New York), 303(5657), 495–499.

Quigley DA, & Kristensen V (2015). Predicting prognosis and therapeutic response from interactions between lymphocytes and tumor cells. Molecular Oncology, 9(10), 2054–2062. [PubMed: 26607741]

Ramakrishnan N, Sunil Kumar PB, & Ipsen JH (2010). Monte Carlo simulations of fluid vesicles with in-plane orientational ordering. Physical Review E, Statistical, Nonlinear, and Soft Matter Physics, 81(4 Pt 1), 041922. [PubMed: 20481768]

Ramakrishnan N, Sunil Kumar PB, & Radhakrishnan R (2014). Mesoscale computational studies of membrane bilayer remodeling by curvature-inducing proteins. Physics Reports, 543(1), 1–60. [PubMed: 25484487]

Ramakrishnan N, et al. (2018). Excess area dependent scaling behavior of nano-sized membrane tethers. Physical Biology, 15(2), 026002. [PubMed: 29116056]

Ramakrishnan N, Tourdot RW, & Radhakrishnan R (2016). Thermodynamic free energy methods to investigate shape transitions in bilayer membranes. International Journal of Advances in Engineering Sciences and Applied Mathematics, 8(2), 88–100. [PubMed: 27616867]

Ramanan V, et al. (2011). Systems biology and physical biology of clathrin-mediated endocytosis. Integrative Biology (Camb), 3(8), 803–815.

Ren G, et al. (2006). The BAR domain proteins: Molding membranes in fission, fusion, and phagy. Microbiology and Molecular Biology Reviews: MMBR, 70(1), 37–120. [PubMed: 16524918]

Roux A, et al. (2010). Membrane curvature controls dynamin polymerization. Proceedings of the National Academy of Sciences of the United States of America, 107(9), 4141–4146. [PubMed: 20160074]

Rubashkin MG, et al. (2014). Force engages vinculin and promotes tumor progression by enhancing PI3K activation of phosphatidylinositol (3,4,5)-triphosphate. Cancer Research, 74(17), 4597–4611. [PubMed: 25183785]

Ruffell B, & Coussens LM (2015). Macrophages and therapeutic resistance in cancer. Cancer Cell, 27(4), 462–472. [PubMed: 25858805]

Safran SA (1999). Curvature elasticity of thin films. Advances in Physics, 48(4), 395–448.

Seifert U (1997). Configurations of fluid membranes and vesicles. Advances in Physics, 46(1), 13–137.

Shibata Y, et al. (2009). Mechanisms shaping the membranes of cellular organelles. Annual Review of Cell and Developmental Biology, 25, 329–354.

Shinohara H, et al. (2017). Regulated polarization of tumor-associated macrophages by miR-145 via colorectal cancer-derived extracellular vesicles. Journal of Immunology, 199(4), 1505–1515.

Sung BH, et al. (2015). Directional cell movement through tissues is controlled by exosome secretion. Nature Communications, 6.

Thomas D, & Radhakrishnan P (2019). Tumor-stromal crosstalk in pancreatic cancer and tissue fibrosis. Molecular Cancer, 18(1), 14. [PubMed: 30665410]

Tourdot RW, et al. (2014a). Multiscale computational models in physical systems biology of intracellular trafficking. IET Systems Biology, 8(5), 198–213. [PubMed: 25257021]

Tourdot RW, et al. (2015). Application of a free-energy-landscape approach to study tension-dependent bilayer tubulation mediated by curvature-inducing proteins. Physical Review E, 92(4).

Tourdot RW, Ramakrishnan N, & Radhakrishnan R (2014b). Defining the free-energy landscape of curvature-inducing proteins on membrane bilayers. Physical Review E, Statistical, Nonlinear, and Soft Matter Physics, 90(2), 022717. [PubMed: 25215768]

Tsai FC, et al. (2021). Comparing physical mechanisms for membrane curvature-driven sorting of BAR-domain proteins. Soft Matter, 17(16), 4254–4265. [PubMed: 33870384]

Vitale I, et al. (2019). Macrophages and metabolism in the tumor microenvironment. Cell Metabolism, 30(1), 36–50. [PubMed: 31269428]

Wang JD, et al. (2017). Clinicopathological significance of SMAD4 loss in pancreatic ductal adenocarcinomas: A systematic review and meta-analysis. Oncotarget, 8(10), 16704–16711. [PubMed: 28053288]

Weigelt B, Peterse JL, Van LJ, & Veer ‘T (2005). Breast cancer metastasis: Markers and models. Nature Reviews Cancer, 5(8), 591–602. [PubMed: 16056258]

Whiteside TL (2016a). Exosomes and tumor-mediated immune suppression. The Journal of Clinical Investigation, 126(4), 1216–1223. [PubMed: 26927673]

Whiteside TL (2016b). Tumor-derived exosomes and their role in cancer progression. Advances in Clinical Chemistry, 74, 103–141. [PubMed: 27117662]

Wollert T, & Hurley JH (2010). Molecular mechanism of multivesicular body biogenesis by ESCRT complexes. Nature, 464(7290), 864–869. [PubMed: 20305637]

Wollert T, et al. (2009). Membrane scission by the ESCRT-III complex. Nature, 458(7235), 172–177. [PubMed: 19234443]

Xu R, et al. (2018). Extracellular vesicles in cancer—Implications for future improvements in cancer care. Nature Reviews Clinical Oncology, 15(10), 617–638.

Yin Y, Arkhipov A, & Schulten K (2009). Simulations of membrane tubulation by lattices of amphiphysin N-BAR domains. Structure (London, England: 1993), 17(6), 882–892. [PubMed: 19523905]

Zhao Y, et al. (2013). Exo70 generates membrane curvature for morphogenesis and cell migration. Developmental Cell, 26(3), 266–278. [PubMed: 23948253]

Zimmerberg J, & Kozlov MM (2006). How proteins produce cellular membrane curvature. Nature Reviews Molecular Cell Biology, 7(1), 9–19. [PubMed: 16365634]

Zimmerberg J, & McLaughlin S (2004). Membrane curvature: How BAR domains bend bilayers. Current Biology, 14(6), R250–R252. [PubMed: 15043839]

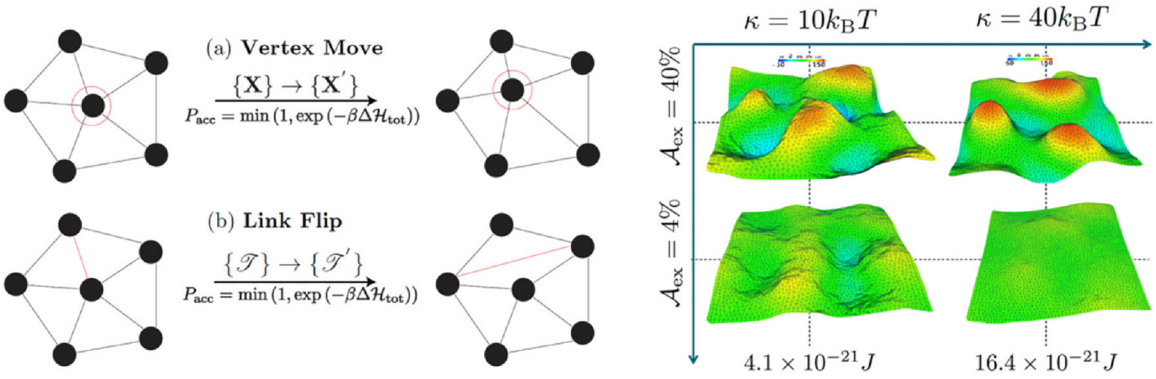

Fig. 1.

(*left*) Dynamical triangulated Monte Carlo scheme to independently modify the position (A) and the connectivity (B) of the vertices in the triangulated surface model. (*right*) Conformations of membranes with different bending stiffness and excess area. Shown are shapes for two values of the excess areas and two different bending rigidities.

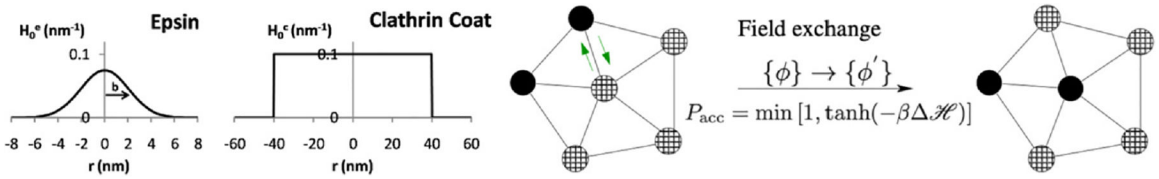

Fig. 2.

(*Left, Middle*) curvature field for epsin and clathrin; (*Right*). Monte Carlo moves for protein migration on membrane.

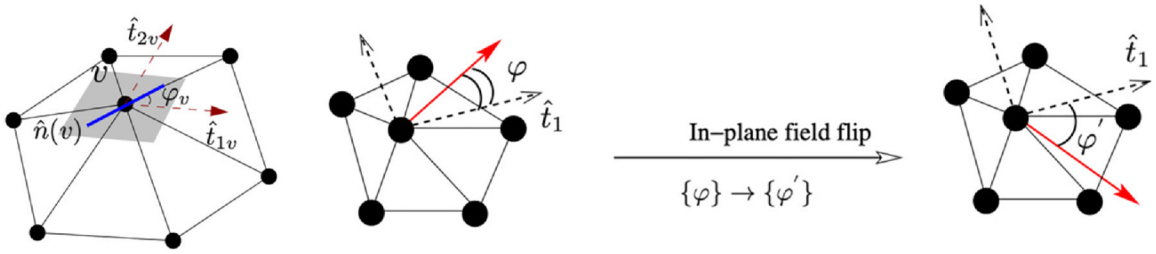

Fig. 3.

(*Left*). Nematic field on a membrane; (*Right*). Flipping the nematic field.

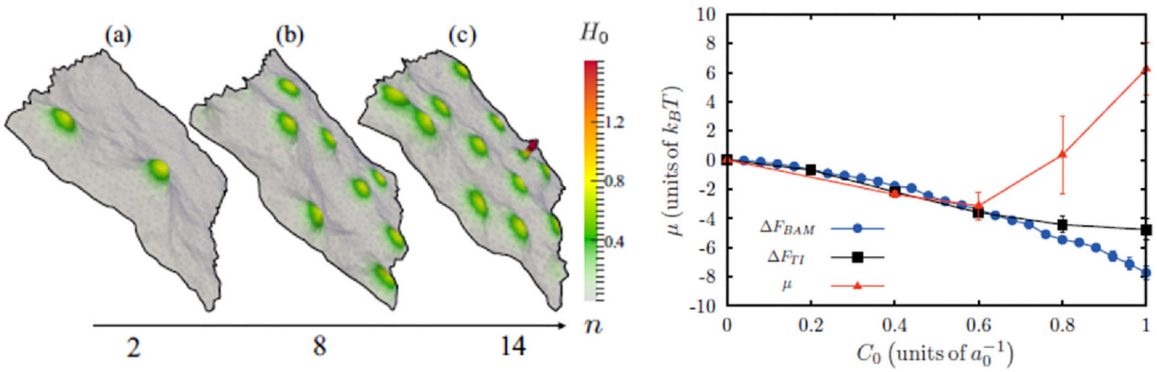

Fig. 4.

(*Left*) onset of tubulation (see panel C) by high density of curvature-inducing proteins; (*Right*) comparison of three free energy methods described in the methods section above showing internal consistency for low to moderate field-strengths. The range of validity covers the biological range of the curvature field strengths, thereby making these methods suitable for biological applications.

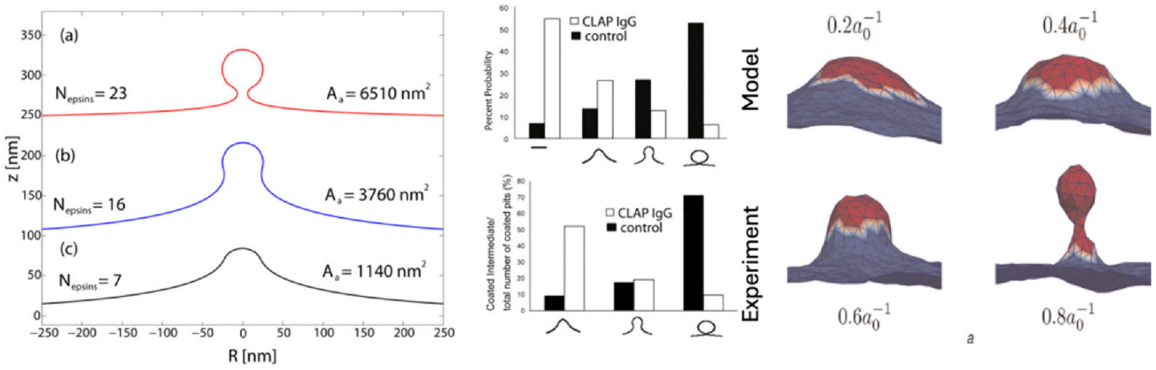

Fig. 5.

(*Left*) membrane deformation profiles under the influence of imposed curvature of the epsin shell model for three different coat areas; here $\kappa = 20k_BT$. For the largest coat area, the membrane shape is reminiscent of a clathrin-coated vesicle. (*Middle*) calculated (top) and experimentally measured (bottom) probability of observing a clathrin-coated vesicular bud of given size in WT cells (filled) and CLAP IgG injected cells (unfilled). (*Right*) vesicle morphologies subject to thermal fluctuations and entropic effects; here $a_0 = I_0$.

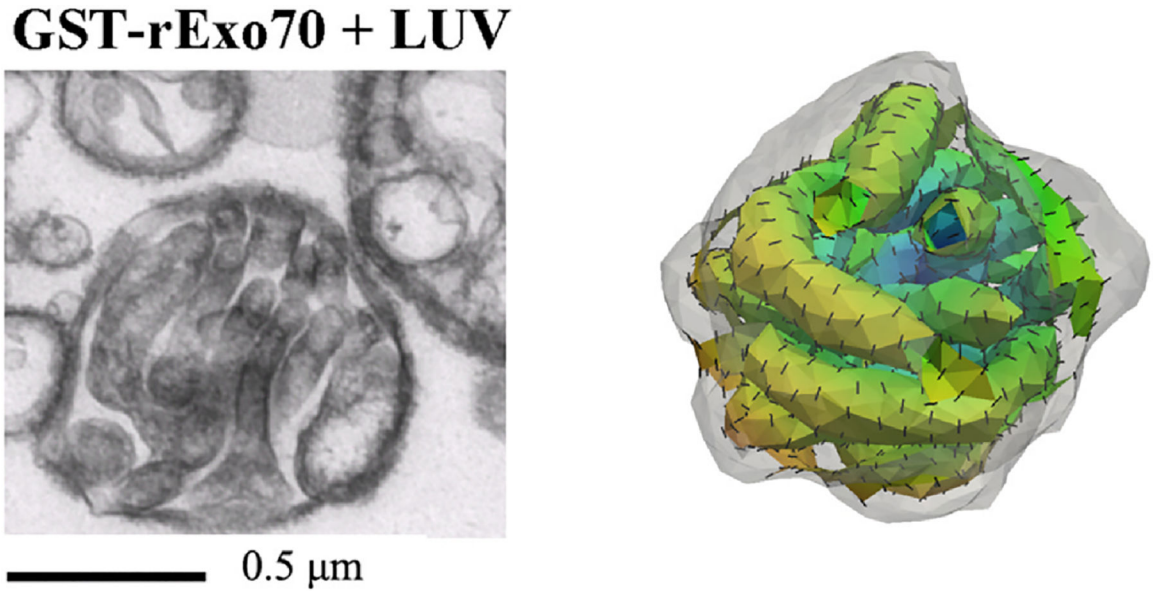

Fig. 6.

(*Left*) experimental observation of Exo70 on GUV and (*Right*) results from the anisotropic curvature model.

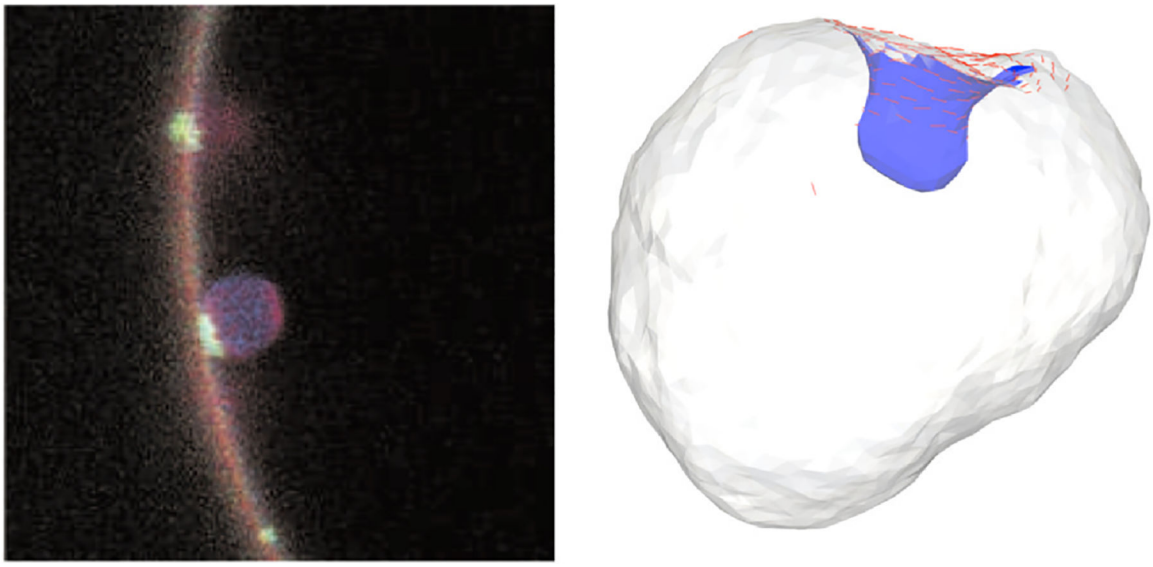

Fig. 7.

(*Left*) Fluorescence image shows the membrane in red and the location of ESCRT proteins in green (Wang et al., 2017). (*Right*) simulation results showing the novel phenomenon of budding by constriction—negative curved bud generated by negatively curved proteins localized to an annular region; the protein field does not localize the area of the bud.

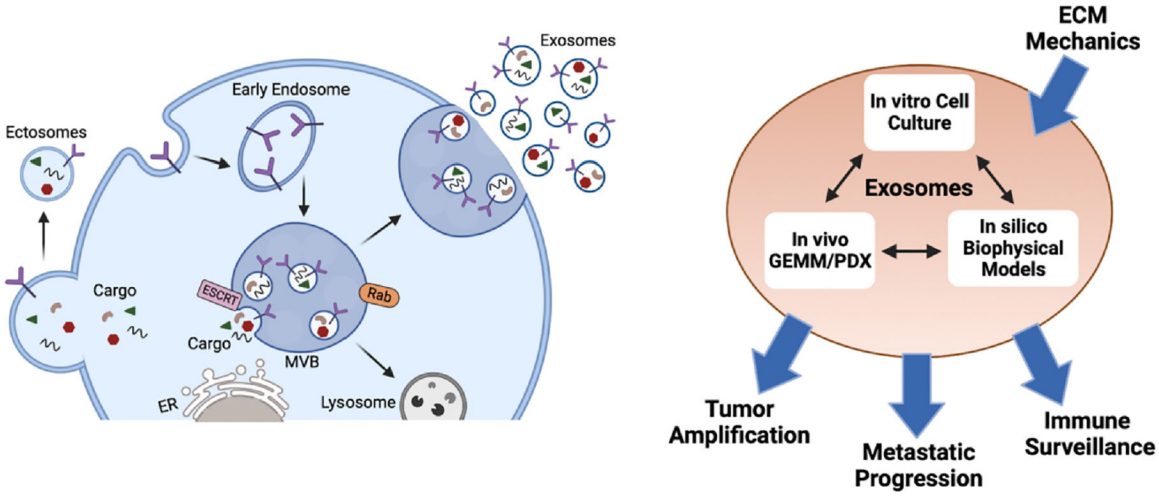

Fig. 8.

(*Left*) Biogenesis and trafficking of exosomes. The ESCRT complexes mediate the invagination of the limiting membrane of endosomes toward the lumen, thereby generating multivesicular endosome (MVEs); MVEs can be transported to the lysosome for breakdown or delivered to the plasma membrane for exosome release. The Rab family of small GTPases are master regulators of endosomal trafficking. Exosomes can carry a variety of proteins, nucleic acids, lipids, and glycans; (*Right*) Implications to fundamental questions in cancer biology and oncology research. How does ECM mechanics and tension sensitive pathways effect exosome production and composition to direct tumor progression and metastasis? *Created with* BioRender.com